JMEPEG (2020) 29:6484–6493
https://doi.org/10.1007/s11665-020-05167-0

1059-9495/$19.00

Preparation and Properties of Zn-Cu Alloy for Potential Stent Material

Jiajun Huang, Yonglai Lai, Hualan Jin, Hongmin Guo, Fanrong Ai, Qi Xing, Xiangjie Yang, and David J. Ross

(Submitted March 25, 2020; in revised form September 4, 2020; published online October 6, 2020)

Among degradable metal cardiac stent materials, zinc has great biocompatibility and corrosion properties, which make it become the most potential stent material. However, the mechanical properties of zinc cannot meet the performance requirements of stent material which severely limit its application. In this paper, Zn-*x*Cu (*x* = 1, 2 and 3 wt.%) alloys were prepared, and their mechanical properties, corrosion properties and biocompatibility were studied. Tensile testing showed the tensile strength and hardness of Zn-*x*Cu alloys both increased with the addition of copper, but the elongation decreased at first and then upturned. Since the formation of galvanic cell, the corrosion rates of Zn-*x*Cu alloys increased. The main corrosion mechanism of Zn-*x*Cu alloy was pitting corrosion, and the corrosion products mainly included ZnO and $Zn(OH)_2$. The cytotoxicity evaluation showed that Cu^{2+} and Zn^{2+} would contribute to cell proliferation, while the concentrations of them reached a suitable range like the concentration of soaking solution of Zn-3Cu alloy was 25%. However, it would inhibit proliferation, while the concentrations of Zn^{2+} and Cu^{2+} were too large. In general, Zn-3Cu alloy had the best comprehensive properties.

Keywords biocompatibility, corrosion rate, mechanical properties, stent, zinc-copper alloys

1. Introduction

Percutaneous coronary intervention as an effective way to cure cardiovascular diseases had received widespread attention. Coronary stent could be divided into permanent stent and degradable stent. According to different types of materials, it also could be divided into metal stent, inorganic nonmetal stent and polymer stent. At now, metal stent is the most commonly used.

Permanent metal cardiac stent materials mainly use titanium and titanium alloys. As applied materials, it has been studied extensively. Eren Yılmaz et al. (Ref 1, 2) researched Ti-Nb alloys and Ti-Nb-*x*Zr alloys. It was founded that the increment of the porosity lowered the corrosion resistance in Ti-Nb alloys and the addition of Zr decreased the grain size and stabilized the β phase in Ti-Nb-*x*Zr alloys. However, due to its non-degradable characteristic, a second operation was required to remove the stent, causing secondary injury to the human body, which turned the focus of researchers to the degradable metal cardiac stent materials.

Jiajun Huang and Yonglai Lai are common first author.

Jiajun Huang, Fanrong Ai, and **Xiangjie Yang**, School of Materials Science and Engineering, Nanchang University, Nanchang 330031, People's Republic of China; **Yonglai Lai, Hualan Jin,** and **Hongmin Guo**, School of Mechanical and Electrical Engineering, Nanchang University, Nanchang 330031, People's Republic of China; **Qi Xing**, Department of Cardiovascular Diseases, Mayo Clinic, Rochester, MN 55905; **David J. Ross**, Department of Biomedical Engineering, Michigan Technological University, Houghton, MI 49931. Contact e-mail: hualanjin@ncu.edu.cn.

Degradable metal cardiac stent materials mainly include magnesium alloys, zinc alloys and iron-based alloys. Magnesium alloys are the most studied degradable metal materials due to their great biocompatibility and degradability. However, the corrosion rates of magnesium alloys in blood are too large to provide sufficient mechanical support and the corrosion products will affect the PH value changes of local physiological tissues. Iron-based alloys are widely used because of their low price and excellent mechanical properties, but the corrosion rates of iron-based alloys are very small. Zinc alloys have good degradation performance and good biocompatibility, which makes them more and more important in recent years.

The standard electrode potential of Zn is − 0.763 V, which is between magnesium (− 2.372 V) and iron (− 0.447 V). Therefore, zinc and its alloys have temperate corrosion resistance. According to reports, Zn alloys have a good corrosion resistance, but it will change with time in human body. Bowen et al. (Ref 3) implanted pure zinc wire into the vascular of rats; on day 45, the degradation rate of pure zinc wire was 0.012 mm/year and increased to 0.05 mm/year on day 180. The microstructure of pure zinc wire after 180 days of implantation was observed; it was found that the Zn wire was uniformly corroded and the corrosion products were mainly ZnO and Zn-containing carbonate. Li et al. (Ref 4) implanted zinc alloy to the medullary cavity of the rats. After 8 weeks, the corrosion rate of the Zn alloy was calculated based on the μ-CT results. As the implantation time increased, the corrosion rates of the alloy were 0.17, 0.19 and 0.22 mm/year, respectively, which were significantly lower than the corrosion rates of Mg and Mg alloy. Normally, the corrosion rate requirement of metal-based degradable material is 0.02 mm/year in average, and the corrosion rate of pure zinc is very close to this figure (Ref 5).

In biocompatibility, Zn alloys also perform well. Zinc is necessary for human growth because it plays an important role in the human body. An adult needs to take about 5 to 20 mg of Zn per day (Ref 6). Schaffer et al. (Ref 7) found that human artery endothelial cells and smooth muscle cells maintained 50%

activity when the concentrations of Zn^{2+} in the soaking solution were 340 and 330 μmol/L. Ma et al. (Ref 6) found that the proliferation rate of coronary endothelial cells increased when the soaking solution with Zn^{2+} concentration was 20 μmol/L, and decreased when the concentration of Zn^{2+} in the soaking solution was 100 μmol/L. Shearier et al. (Ref 8) found that the activities of human vascular endothelial cells, human arterial smooth muscle cells and human skin fibroblasts reached 50% when the concentrations of Zn^{2+} in the corresponding soaking solution were 265, 70 and 50 μmol/L, respectively. When these cells directly contacted the surface of Zn alloy, the cells survived very well at first, and then, apoptosis occurred very quickly. However, the cells could grow well on the Zn surface which had subjected to a certain surface treatment. Bowen et al. (Ref 9) implanted pure Zn filaments into the blood vessels of mice and found that zinc and zinc degradation products did not cause inflammatory reactions, and could inhibit smooth muscle cells proliferation and vascular restenosis. The animals did not show poisoning phenomenon in whole body or local tissue during the experiment. At the same time, the results obtained by the hemolysis test showed that the hemolysis rates of Zn and different Zn-based alloys were less than 5% and the platelets could adhere well to the surface of the Zn alloy, which indicated that Zn and Zn alloys had great blood compatibility and did not cause blood vessels to form thrombus. Murni et al. (Ref 10) found that the cell activity of osteoblasts in the extract of Zn-3 mg decreased by 50% on the first day, but rallied on the 3rd and 7th day. This meant that the activity of the cells may gradually recover over time.

The mechanical properties of pure Zn are not good, but it can be strengthened by adding alloying elements and heat treatment. Alloying elements need to consider its biocompatibility, so the alloying elements which are innocuous to the human body are selected. Therefore, the addition of elements such as Mg, Cu, Ca and Mn to the degradable Zn-based alloy has become the preferred direction of research. M. Sikora-Jasinska et al. (Ref 11) found that increase in Ag content monotonically improved tensile strength due to grain refinement and a higher volume fraction of $AgZn_3$ particles at room temperature, and the ductility loss was found to be independent of Ag content. Many studies have proven that the addition of alloying elements can indeed improve the mechanical properties of zinc.

As a trace metal element, copper plays an important role in maintaining the health of the human cardiovascular system. A variety of cardiovascular diseases, such as hypertension, coronary heart disease and arrhythmias, have been proven that associate with copper deficiency. Therefore, the intake of copper is very necessary for human. In terms of biological mechanism, copper is so important because it can affect the formation and physiological functions of blood vessels. Copper is involved in the synthesis and expression of related factors in angiogenesis and affects vasodilation by the action of NO (Ref 12). A variety of biomedical materials containing copper have been proven that accelerate the formation of blood vessels by releasing copper ions. An experiment has shown that copper-containing coronary stent materials can promote the proliferation and migration of endothelial cells, which is expected to reduce the incidence of in-stent restenosis and thrombosis (Ref 13). These advantages make Zn-Cu alloys have great prospects in biodegradable cardiovascular scaffold materials.

Zinc-copper alloys have a peritectic reaction at 424 °C, $L + \varepsilon(CuZn5) = \eta(Zn)$. Therefore, in this experiment the alloy compositions were selected mainly in the $\varepsilon + \eta$ two-phase region for detecting the effect of second phase, and one composition was selected in the η single-phase region for detecting effect of solid solution, so Zn-xCu (x = 1, 2, 3 wt.%) alloys were prepared. In order to make the alloy meet the requirement in mechanical properties, corrosion performance and biocompatibility, this study researches the effects of Cu content on the performance of these aspects of the alloys. The main purpose of this paper is to explore the mechanism and law of mechanical, corrosion and biocompatibility performance by adding copper to zinc, compare these aspects of performance and obtain the best comprehensive performance of Zn-xCu alloy for the future study and application.

2. Experimental Procedure

2.1 Materials Preparations

The Zn-xCu alloys (x = 1, 2 and 3 wt.%, denoted as Zn-1, 2, 3 Cu, respectively) were cast by pure zinc (99.99 wt.%) and pure copper (99.99 wt.%). Pure zinc bulks were put into the well type melting furnace and heated to 200 °C for 30 min to dry, then continued to heat to 550 °C for 90 min, while copper powder was added into crucible. After alloys were melted, the alloy liquid was stirred with a graphite rod to make the composition uniform and then skimmed the slag. While the alloy liquid cooled to 500 °C, poured it into a stainless steel mold to obtain a sample. The as-cast mold homogenized annealed at 300 °C for 12 h and then cooled in oven. For soaking and cell compatibility test, samples (Φ16 mm × 5 mm and 10 mm × 10 mm × 3 mm) were cut from the rods, polished and then ultrasonically cleaned in ethanol.

2.2 Microstructure Characterization

The alloy compositions were analyzed by using the inductive coupling plasma emission spectrograph (ICP, Elmer Optima 8000, USA). Microstructures of as-cast and heat-treated samples was observed by metallographic microscope (OM, shunyuRX50M, china), and all samples were polished and then etched with an acid solution (4% nitric acid in absolute ethanol). The phase compositions were detected by x-ray diffraction analyzer (XRD, Rigaku SmartLab, Japan). The tensile fracture of the samples were observed by using a scanning electron microscope (SEM, FEI Quanta FEG 250, US) (Fig. 1).

2.3 Mechanical Performance Test

The stretching tests were experimented on a Meites Industrial System E45.105 electronic universal testing machine with the tensile rate of 1 mm/min, and three parallel samples of each heat-treated alloy. According to the national standard GB/T228-2002 ''metal material stretching test method,'' this experiment uses the proportion specimen, the proportional coefficient is 5.65, and the specific size is shown in Fig. 2.

The hardness tests were experimented on a Nanjing Shant HXS-1000A digital intelligent micro-Vickers hardness tester.

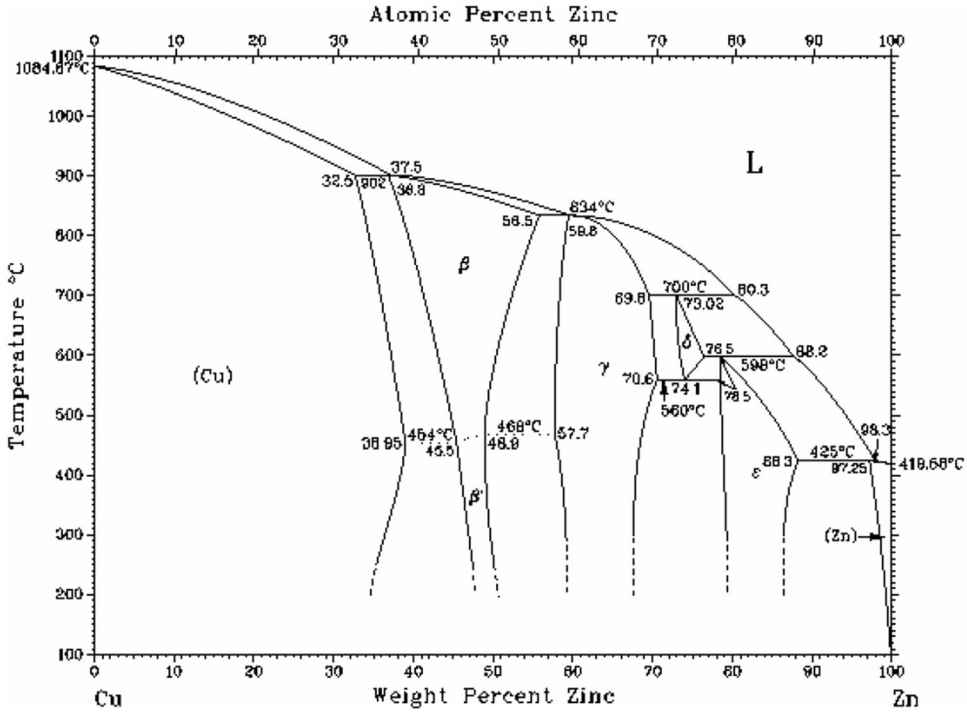

Fig. 1 (Ref 14) Zn-Cu alloy binary phase diagram

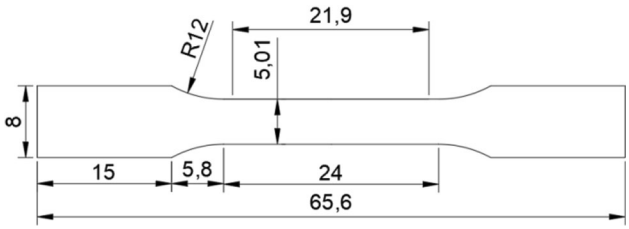

Fig. 2 Dimensional drawing of tensile specimen

The samples were ground, polished and etched before testing. The applied load was 200 N, the loading time was 15 s, and each sample was tested at 5 points and averaged.

2.4 Corrosion Properties Test

Electrochemical experiments were experimented in HANKS simulated body fluids. The heat-treated samples were made into 10 mm × 10 mm × 3 mm cuboids, ground with sandpaper, polished and immersed into HANKS simulated body fluids. The reference electrode was a calomel electrode, and the auxiliary electrode was a platinized platinum electrode. Using a Koster CS electrochemical workstation, the scan rate was 0.001 V/s and the scan range was 4 to − 4 V. The corrosion morphology after electrochemical experiments was observed using SEM equipped with EDS.

Corrosion rates were estimated in terms of penetration rate (CR) using the Faraday's laws (Ref 15):

$$\mathrm{CR} = K_1 \frac{i_{\mathrm{corr}}}{\rho} \mathrm{EW}$$
$$\mathrm{EW} = \frac{1}{\sum \frac{n_i f_i}{w_i}} \qquad \text{(Eq 1)}$$

where CR is the corrosion rate (mm/year), i_{corr} is the corrosion current density (A/cm^2), $K_1 = 3.27 \times 10^3$ mm g/A × cm × year, ρ is the density (g/cm^3), EW is the equivalent weight of the alloy, f_i = the mass fraction of the ith element in the alloy, w_i = the atomic weight of the ith element in the alloy, and n_i = the valence of the ith element of the alloy.

The immersion tests were experimented in a beaker containing HANKS simulated body fluids. The samples size was Φ16 mm × 5 mm. After ground, polished and immersed, the samples into the HANKS simulated body fluid. The HANKS simulated body fluids would be changed every 24 h. After sometimes, the sample was taken out, washed by deionized water, blown dry and weighed.

The corrosion rate is calculated as (Ref 15): CR = 8.76 × $10^4(W_1 - W_2)/A \times T \times D$ mm/year, where: CR is corrosion rate (mm/year), A is surface area before sample immersion (cm^2), T is immersion time (h), D is sample density (g/cm^3), W_1 is sample weight before corrosion, and W_2 is sample weight after corrosion.

2.5 Cytotoxicity Evaluation

Biocompatibility experiments were experimented in the heat-treated Zn-Cu alloy soaking solution. First, the surface of the alloy was ground and cleaned to remove impurities, and then, the alloy was sterilized and sterilized by ultraviolet irradiation. The alloy was immersed in the soaking solution for one day, and then diluted to obtain the Zn-Cu alloy soaking solutions which had the concentration of 100, 50, 25, 12.5 and 6.25% of the original concentration. After SD rat bone marrow mesenchymal cells had cultured in the cell culture chamber for 2-3 generations, SD rat bone marrow mesenchymal cells were inoculated into different concentrations of Zn-Cu alloy extract for 1 day. Thecck-8 reagents were used to observe the number of cells. The cell proliferation rate was obtained by comparing

the number of cells surviving in the soaking solution and the soaking solution without Zn-Cu alloy soaking.

Cytotoxicity was evaluated according to the relative cell proliferation rate of cells; the relative cell proliferation rate of cells is calculated as: Relative cell proliferation rate (Ref 16) = $OD_{sample}/OD_{control\ group} \times 100\%$. When the relative cell proliferation rate belong to $\geq$ 100% was grade 0; 75-99% was grade 1; 50-74% was grade 2; 25-49% was grade 3; 1-24% was grade 4, and 0% was grade 5. Grade 0-1 was qualified, and grade 3-5 was unqualified (Table 1).

3. Results and Discussion

3.1 Actual Alloy Composition of Zn-xCu

In the smelting process, it was difficult to obtain the same alloy composition as expected due to burning loss, slag skimming and so on. Therefore, the actual composition of the alloy was tested in this experiment. The actual composition of the alloy is shown in Table 2.

3.2 Microstructure Characterization

Figure 3 is an XRD diffraction pattern of Zn-*x*Cu alloys. The results show that the Zn-1Cu alloy has the η phase and a little number of the ε phase (maybe because of the non-equilibrium solidification) and the Zn-2Cu and Zn-3Cu alloys have the obvious η phase and ε phase, which suggest that with the Cu content increasing, the number of the ε phase increases significantly.

The above conclusions can also be drawn from the following figures. The microstructure of pure Zn (Fig. 4a) and Zn-1Cu alloy (Fig. 4c) is named as pure Zn matrix and primary Zn matrix, respectively. There is no second phase in the primary zinc matrix obtained by combining copper atom with zinc atom lattice, and the grain boundary is reticulated and rich in Cu atoms. It can be seen from Fig. 4(b) and (d) that the η phase grains of Zn and Zn-1Cu alloys grow obviously after heat treatment. In the process of homogenization annealing, the Cu atoms at the grain boundary were diffused, which made the grain boundary of Zn-1Cu clearer and the enrichment disappeared. The microstructure of Zn-2Cu alloy (Fig. 4e) and Zn-3Cu alloy (Fig. 4g) is dendritic phase which distributes on the primary zinc matrix. As the Cu content increased, the number of ε phase increased and the ε phase arm spacing decreased. After the heat treatment, the amount of the second phase was reduced because the alloy composition was uniform.

3.3 Mechanical Properties

As can be seen from Table 3, changes in the copper content have a significant effect on the mechanical properties of the heated treated zinc-copper alloy. As the copper content increases, the strength of the alloy also increases significantly. According to the microstructure, the change in mechanical properties of the Zn-Cu alloy can be explained. The increase in the strength of the Cu-1Zn alloy compared to the pure zinc due to the strengthening of solid solution. Cu-2Zn and Cu-3Zn alloys precipitated a brittle second phase (ε phase), while Cu-3Zn alloys had more second phase than Cu-2Zn alloys. Both

Table 2 Zn-*X*Cu alloy ICP results

	Zn-1Cu	Zn-2Cu	Zn-3Cu
Cu (wt.%)	0.72	1.64	2.43
Burn rate (%)	28%	18%	19%

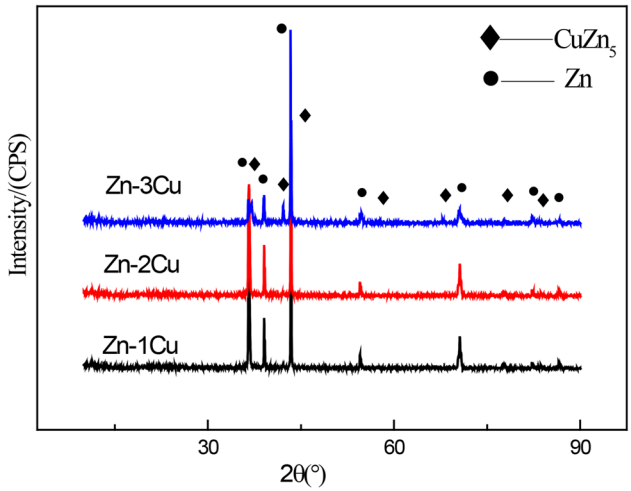

Fig. 3 XRD diffraction patterns of alloys with different compositions

Table 1 Comparison of properties of different zinc-based alloys

Alloys	Tensile strength, MPa	Elongation, %	References
Zn-1 Mg	265	8.3	(Ref 4)
Zn-1Ca	240	7.8	(Ref 4)
Zn-1Sr	262	10.3	(Ref 4)
Pure Zn (hot extruded)	61	3.8	(Ref 15)
Zn-1Cu (hot extruded)	186.3	21	(Ref 15)
Zn-2Cu (hot extruded)	240	46.8	(Ref 15)
Zn-3Cu (hot extruded)	257	47.02	(Ref 15)
Zn-4Cu (hot extruded)	270	50.6	(Ref 15)
Mg-RE-based alloys	233	25.9	(Ref 17)
Mg-6Zn	279.5	18.8	(Ref 18)

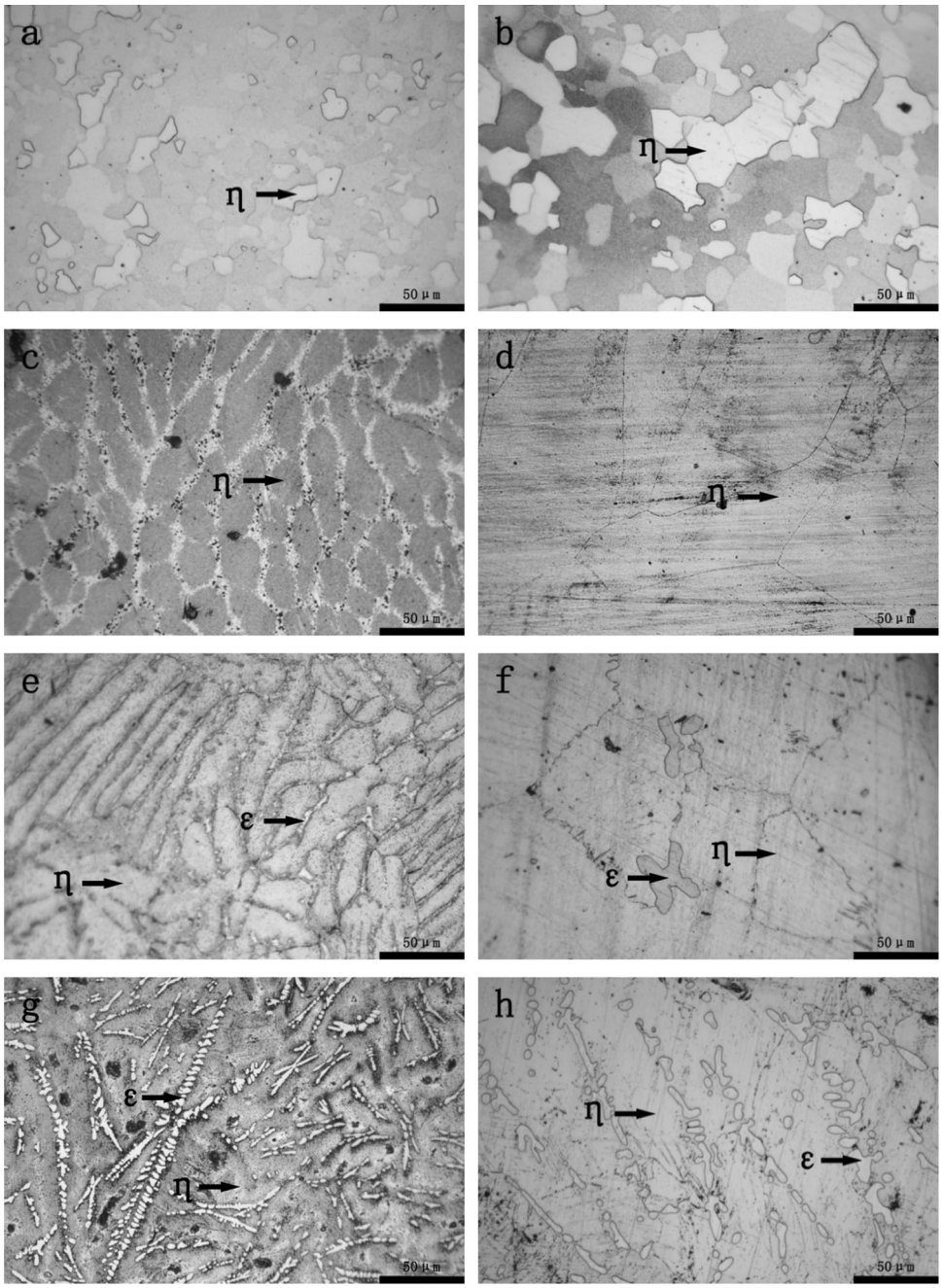

Fig. 4 Photomicrographs of alloys with different compositions: (a) as-cast Zn; (b) heat-treated Zn; (c) as-cast Zn-1Cu; (d) heat-treated Zn-1Cu; (e) as-cast Zn- 2Cu; (f) heat-treated Zn-2Cu; (g) as-cast Zn-3Cu; (h) heat-treated Zn-3Cu

Table 3 Mechanical properties of the heat-treated Zn-*x*Cu alloys with different compositions

	Zn	Zn-1Cu	Zn-2Cu	Zn-3Cu
Tensile strength (MPa)	6.68 ± 0.18	19.20 ± 0.61	68.50 ± 1.91	105.5 ± 4.43
Elongation (%)	8.17 ± 0.27	1.70 ± 0.05	2.77 ± 0.04	4.06 ± 0.14
Micro-Vickers hardness (HV)	34.30 ± 0.68	61.72 ± 1.29	68.78 ± 1.71	76.64 ± 1.76

the solid solution and the second phase hinder the movement of dislocations, which leads to the improvement of the strength of the alloy. Similarly, the hardness of the alloy increases from 34 to 76.64 HV due to the strengthening of solid solution and

second phase. According to previous studies (Ref 19), the addition of Cu and Mg can significantly refine the grain size. But in this study, this phenomenon did not appear clearly. Maybe the refinement required the synergy of magnesium and copper (Fig. 5).

The crystal structure of zinc is closely packed hexagonal structure with few slip systems and poor plasticity. It can be seen from Table 3 that the elongation of Zn-*x*Cu alloy decreases at first and then increases with the increase in copper content. Because the movement of dislocations was hindered by solid solution firstly, the plasticity of Zn-1Cu was lower. Then, after Cu was continuously added, the formed second phase was easily separated from the interface of the substrate and became a crack source. At this time, the fracture mechanism changed from cleavage fracture to quasi-cleavage fracture, which led to the improvement of material plasticity. In addition, macroscopic plastic fracture was observed in pure zinc tensile samples, while the fracture mechanism of the Zn-*x*Cu alloy was brittle fracture.

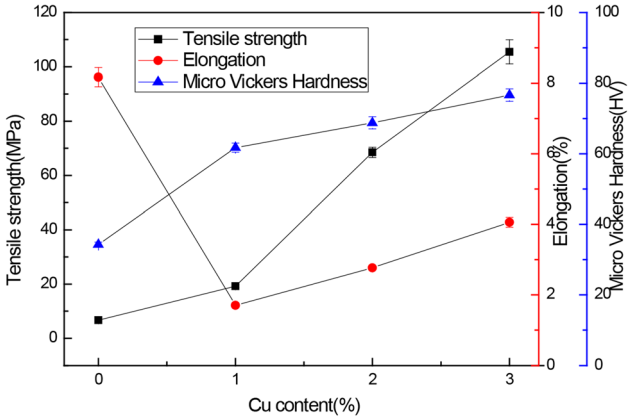

Fig. 5 Mechanical properties of the heat-treated alloys with different compositions

Figure 6 shows the tensile fracture morphology of the heated treated zinc alloy. It can be seen from Fig. 6a and (b) that the fracture of pure zinc and Zn-1Cu alloy is cleavage fracture. There are some smooth grains which are ladder-shaped on the tensile fracture surface, which is a typical cleavage fracture feature. The main cleavage plane is {0001}, and the secondary dissociation surface is {00-24}. Cleavage fracture is a collection of many cleavage facets, which shine under the action of external light source. Figure 6(c) and (d) indicates that the Zn-2Cu and Zn-3Cu alloys exhibited the characteristics of quasi-cleavage fracture. In addition to the cleavage facets, there are some holes. These holes are the sources of cracks formed by the detachment of the second phase particles and are surrounded by cracks formed by crack propagation. Those adjacent cleavage facets join to form a tear ridge.

3.4 Corrosion Performance

Figure 7 is the polarization curves of the heated treated Zn-*x*Cu alloys, and Table 4 shows electrochemical parameters obtained by a polarization curves. It can be seen from Table 4 that the corrosion potential decreases slightly from − 1.312 to − 1.389 V, and the corrosion current increases significantly from 0.0851 to 0.274 mA/cm^2. This phenomenon indicates that corrosion tendencies of zinc-*x*Cu alloys are basically the same, but once corrosion occurs, the corrosion rate of Zn-Cu alloy will increase with the increase in copper content. This result is some different from the hot-rolled state obtained by Tang et al. (Ref 12), which showed no significant difference among Zn-*x*Cu alloys. It can be seen from the polarization curve that Zn-

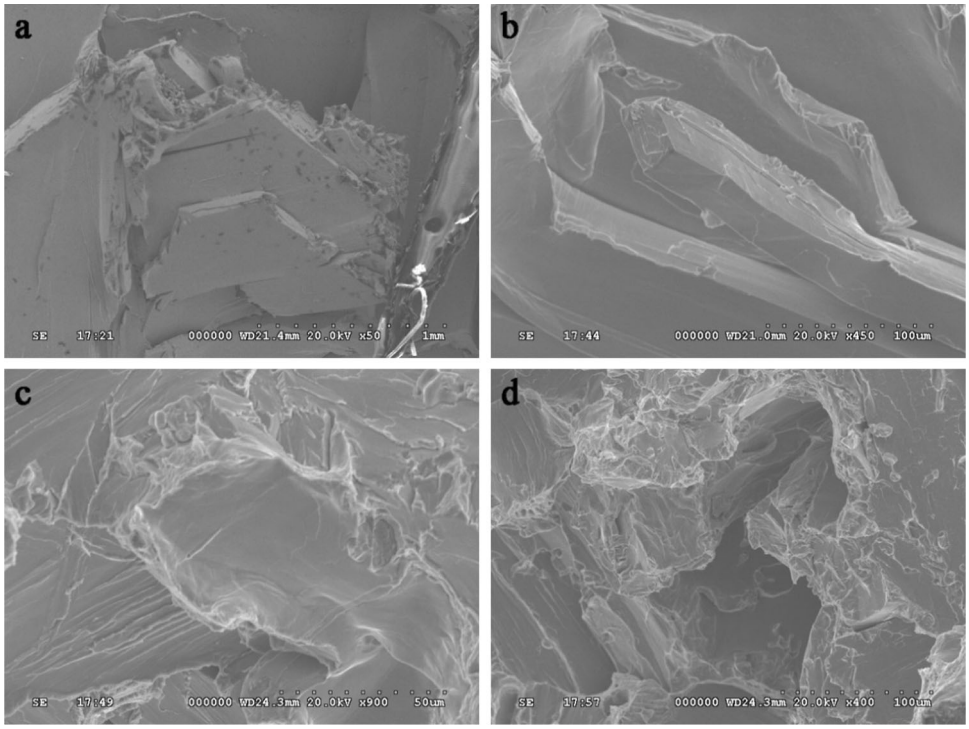

Fig. 6 SEM photomicrographs of tensile fracture of the heat-treated alloys: (a) Zn; (b) Zn-1Cu; (c) Zn-2Cu; (d) Zn-3Cu

Cu alloys conform to Tafel's law and have no obvious passivation behavior, because a large amount of Cl^- can damage the protective film formed by the corrosion products in body fluid.

According to the theory of mixed potentials, because Cu has a higher electrode potential, the addition of Cu will increase the corrosion potential of Zn alloys, but the actual situation is exactly the opposite. This may be due to galvanic corrosion of alloys due to the presence of the second phase. The second phase acts as the cathode and the matrix phase acts as the anode, which accelerates the corrosion of the zinc alloys. In addition, the reason why the corrosion resistance of Zn-1cu is worse than that of Zn may be that the hydrogen evolution overpotential of Cu is low and the exchange current density of hydrogen evolution reaction is high, so the corrosion rate increases sharply.

3.5 Electrochemical Corrosion Degradation Behavior

Figure 8 is the corroded surface of the heated treated Zn-*x*Cu alloy after electrochemical test. From Fig. 8(a), it can be seen that pure zinc has the characteristics of uniform corrosion, and the degree of corrosion is relatively light. The Zn-*x*Cu alloy shows the characteristics of local corrosion in Fig. 8(b), (c) and (d), but the corrosion pittings are evenly distributed on the surface of the alloy. The degree of corrosion becomes intensified with the increase in Cu content, and the accumulation of corrosion products increases, which is consistent with the results obtained by the previous electrochemical experiments. As showed in Fig. 8(e), the corrosion products in Zn-1Cu mainly contain Zn and O, and also a small amount of P, C, Ca and Cu. It is speculated that the main corrosion products are ZnO and $Zn(OH)_2$, and there may be a small amount of $ZnCO_3$ and $Zn_3(PO_4)_2$.

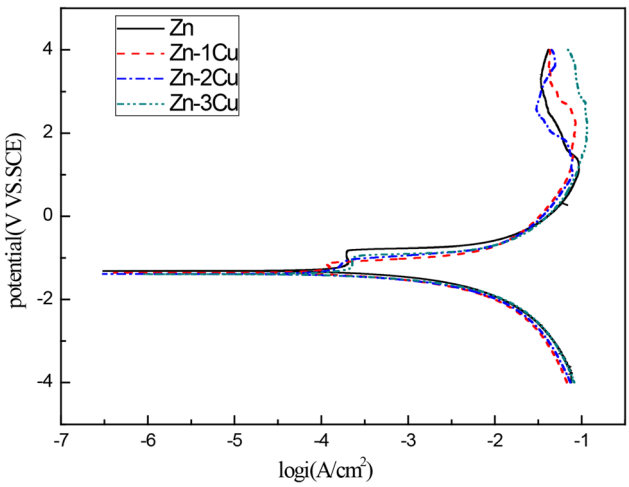

Fig. 7 Electrochemical polarization curves of the heat-treated alloys with different compositions

According to the scanning results of Zn-3Cu (Fig. 8f), the secondary dendritic phase is confirmed as CuZn5. It can be seen from Fig. 8(g) that the secondary dendritic phase which is rich of Zn and Cu elements is relatively intact in the case of electrochemical corrosion. CuZn5 phase was protected as a cathode in galvanic corrosion, resulting in corrode the surrounding anode matrix, and the corrosion products surrounded the CuZn5 phase. As the Cu content increased, the amount of CuZn5 phase also increased, leading to intensified corrosion of the surrounding matrix and increased corrosion products.

3.6 Electrochemical Corrosion Degradation Mechanism

When HANKS simulated body fluid contacted with Zn matrix, the Zn-*x*Cu alloy underwent an electrochemical corrosion, and the body fluid acted as the electrolyte. The CuZn5 phase was protected as the cathode, and the Zn matrix surrounding the CuZn5 phase was dissolved as the anode. The electrochemical reaction equations are as follows:

$$\text{Anode reaction}: \quad Zn \rightarrow Zn^{2+} + 2e^- \qquad \text{(Eq 2)}$$

$$\text{Cathodic reaction}: \quad 2H_2O + O_2 + 4e^- \rightarrow 4OH^- \qquad \text{(Eq 3)}$$

$$\text{General reaction}: \quad 2Zn + 2H_2O + O_2 \rightarrow 4Zn(OH)_2 \qquad \text{(Eq 4)}$$

$Zn(OH)_2$, as a corrosion product covering the surface of the alloy, could play a certain protective role. However, Cl^- existing in the physiological environment would react with $Zn(OH)_2$, breaking the balance between the generation and dissolution of $Zn(OH)_2$. The equation is as follows.

$$6Zn(OH)_2 + Zn_2 + +2Cl^- \rightarrow 6Zn(OH)2 \cdot ZnCl_2 \qquad \text{(Eq 5)}$$

The dissolution of $Zn(OH)_2$ would reduce the protected area on the alloy surface, thereby exposing more fresh surface, and resulting in cyclic galvanic corrosion. As the galvanic corrosion deepened, the matrix surrounding the CuZn5 phase continued to be dissolved, showing obvious pitting corrosion characteristics. In addition, since the simulated body fluid contained a small amount of phosphate ions, carbonate ions and calcium ions, there may also be a small amount of phosphate and carbonate in the corrosion products, which were confirmed in EDS.

In the immersion weight loss test, the corrosion rate curve was calculated by formula in immersion tests part, as shown in Fig. 9. The corrosion test results are basically consistent with the electrochemical test results. The corrosion rate of pure zinc is the lowest, and the corrosion rate of zinc-copper alloy increases gradually with the addition of copper.

Table 4 Electrochemical parameters of the heat-treated alloys with different compositions

	Zn	Zn-1Cu	Zn-2Cu	Zn-3Cu
Corrosion potential (V)	− 1.312	− 1.357	− 1.386	− 1.389
Corrosion current (A/cm^2)	0. 85 × 10^{-6}	1.63 × 10^{-6}	1.90 × 10^{-6}	2.74 × 10^{-6}
Corrosion rate (mm/year)	0.0127	0.0245	0.0228	0.042

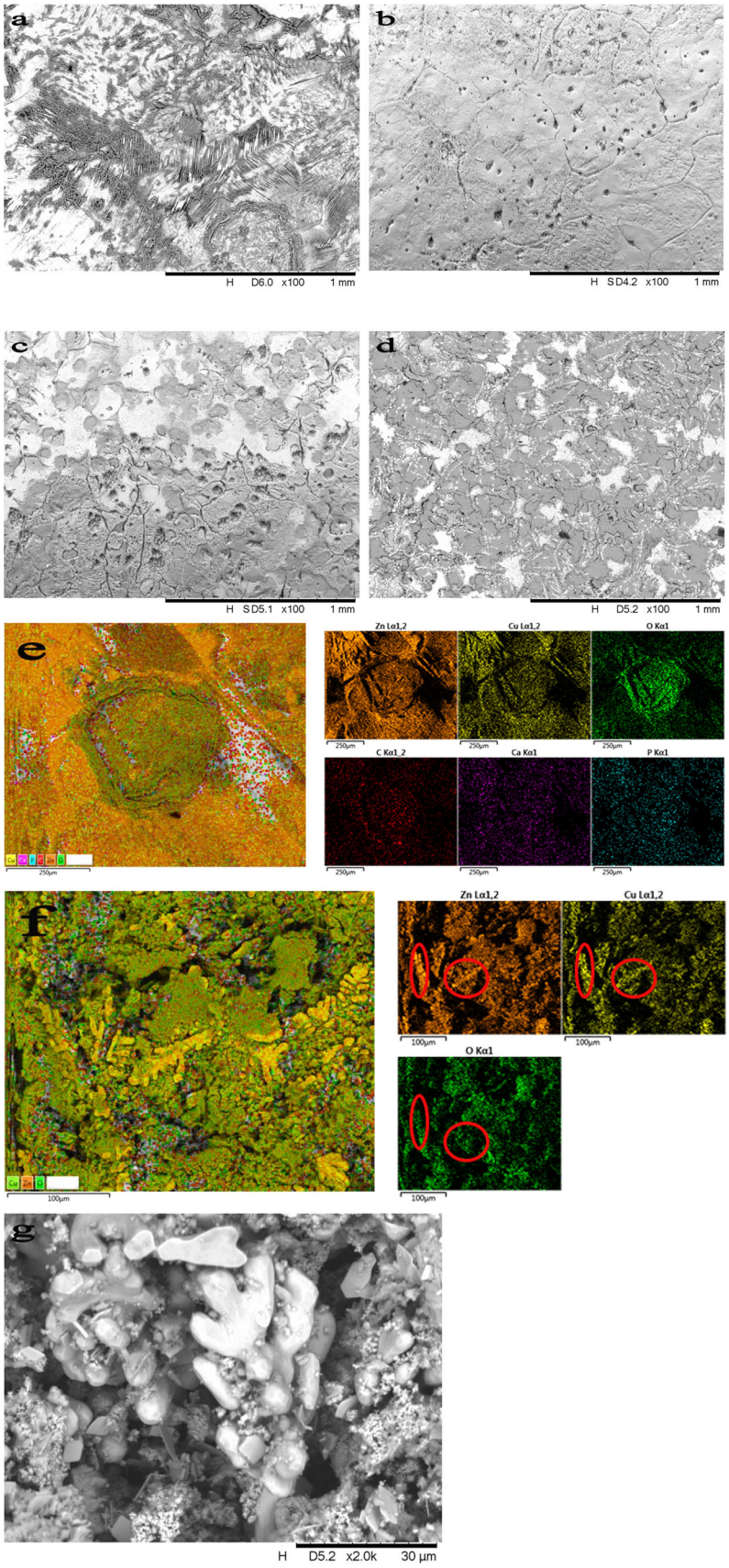

Fig. 8 SEM photomicrographs of corrosion surface of the heat-treated alloys: (a) Zn; (b) Zn-1Cu; (c) Zn-2Cu; (d) Zn-3Cu; (e) surface scan of Zn-1Cu; (f) surface scan of Zn-3Cu; (g) higher multiple Zn-3Cu

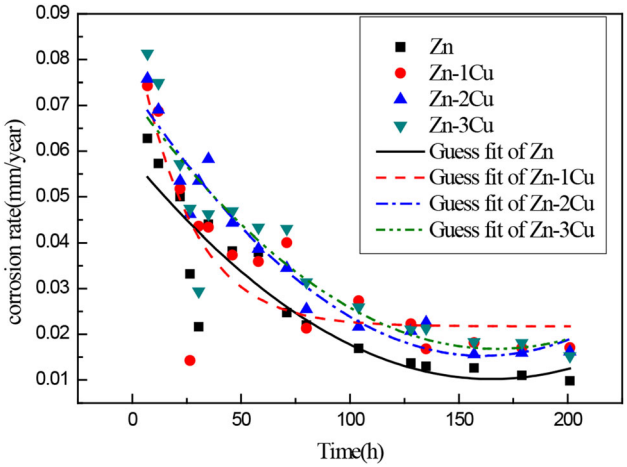

Fig. 9 Curves of immersion corrosion rate of the heat-treated alloys

Table 5 Relative cell proliferation rates of different concentrations of the heat-treated Zn-*x*Cu alloy

c	Zn	Zn-1Cu	Zn-2Cu	Zn-3Cu
100%	35.24%	32.16%	31.26%	29.54%
50%	93.93%	74.16%	30.80%	99.47%
25%	93.31%	92.68%	104.21%	106.20%
12.50%	98.23%	96.19%	102.29%	103.31%
6.25%	91.39%	96.26%	98.66%	99.07%

3.7 Biocompatibility

Table 5 shows the relative cell proliferation rates of different concentrations of the heated treated Zn-Cu alloys soaking solution. It can be seen from Table 5 that the cytotoxicities are all Grade 3 when the concentrations of the Zn-*x*Cu alloys soaking solution are 100%. As the concentration of the soaking solution decreases, the cytotoxicity gradually decreases from the Grade 3 to Grade 1. With the increase in Cu content, the relative cell proliferation rate of Zn-*x*Cu alloy soaking solution with the same concentration also increases. When the concentration of soaking solution of Zn-3Cu alloy is 25%, the relative cell proliferation rate reaches the maximum and the cytotoxicity is grade 0. Wang et al. (Ref 20) declared that for Mg-based alloys, a minimal 6 times to maximal 10 times dilution of extracts could better simulate the in vivo environment. So when the concentration of the Zn-*x*Cu alloys soaking solution are 12.50%, it could be better simulate the body environment. In this situation, Zn-2Cu alloy and Zn-3Cu alloy are Grade 0.

The results show that the concentrations of Zn^{2+} in the soaking solution are too high when the concentration of soaking solution of Zn-*x*Cu alloys is 100%. A research (Ref 19) showed that the addition of Cu and Mg can increase the Zn^{2+} release compared with pure Zn, so the proliferation rates of Zn-*X*Cu alloys decreased with the increase in Cu because of the high concentration of Zn^{2+}. The above results could be attributed to the formation of galvanic micro-cells in the Zn-based alloy, accelerating the corrosion of Zn matrix.

As the soaking solution diluted, the concentration of Zn^{2+} decreased and reached a suitable concentration for cell proliferation. Therefore, the relative cell proliferation rate in the pure zinc soaking solution first increases with the concentration of the soaking solution decreases and then falls back because the concentration of Zn^{2+} is too small, which prove that Zn^{2+} is beneficial to cell proliferation in a suitable range. The addition of Cu^{2+} causes the cytotoxicity with the same concentration of the soaking solution to increase then decrease, which indicates that the cell proliferation can be promoted only when the concentration of Cu^{2+} in a suitable concentration range.

4. Conclusion

This paper studies the effects of copper on the mechanical properties, corrosion properties and biocompatibility of Zn-*x*Cu (X = 0, 1, 2, 3) alloy by heat treated were investigated.

It is concluded that:

1. The presence of the solid solution and the second phase affect the mechanical properties and corrosion properties of the material, which increases the strength from 6.68 to 105.5 Mpa and hardness from 34.3 to 76.64 HV, and the elongation decreases from 8.17 to 1.7% at first and then rallies to 4.06%.
2. Corrosion resistance gets worse due to the formation of galvanic cell. The corrosion rate increases from 0.0127 mm/year to 0.042 mm/year.
3. The main corrosion mechanism of Zn-*x*Cu alloy is pitting corrosion, and the corrosion products mainly include ZnO and $Zn(OH)_2$.
4. Cell proliferation can only be promoted when the Cu^{2+} concentration and Zn^{2+} concentration in the body fluid reach a suitable range. When the concentration of soaking solution of Zn-3Cu alloy was 25%, the cell proliferation is 106.20%.
5. From a comprehensive, performance perspective, Zn-3Cu has the certain corrosion properties, and best mechanical properties and biocompatibility.

Acknowledgments

The National Natural Science Foundation of China (Grant numbers #51401101) is acknowledged for funding this work. & represented these authors contributed equally to this work.

References

1. E. Yılmaz, A. Gökçe, F. Findik, O. Gulsoy, and O. Iyibilgin, Mechanical Properties and Electrochemical Behavior of Porous Ti-Nb Biomaterials, *J. Mech. Behav. Biomed. Mater.*, 2018, **87**, p 59–67
2. E. Yılmaz, A. Gökçe, F. Findik, and O. Gulsoy, Assessment of Ti-16Nb-*x*Zr Alloys Produced Via PIM for Implant Applications, *J. Therm. Anal. Calorimet.*, 2018, **134**(1), p 7–14
3. P.K. Bowen, J. Drelich, and J. Goldman, Zinc Exhibits Ideal Physiological Corrosion Behavior for Bioabsorbable Stent, *Adv. Mater.*, 2013, **25**(18), p 2577
4. H.F. Li, H.X. Xie, Y.F. Zheng, F.Y. Zhou, K.J. Qiu, X. Wang, S.H. Chen, L. Huang, L. Tian, and L. Qiu, Development of Biodegradable

Zn-X Binary Alloys with Nutrient Alloying Elements Mg, Ca and Sr, *Sci. Rep.*, 2015, **5**, p 10719
5. X.W. Liu, *Study on the Structure and Properties of Medical Degradable Zinc-Based Materials*, Harbin Engineering University, Harbin, 2016
6. C. Shen, *Study on Mechanical Properties, Degradation Properties and Biocompatibility of Medical Degradable Zinc Alloy (Zn-1.2 Mg-0.1Ca)*, Fourth Military Medical University, Xi'an, 2017
7. J. Ma, N. Zhou, and D. Zhu, Endothelial Cellular Responses to Biodegradable Metal Zinc, *ACS Biomater. Sci. Eng.*, 2016, **2**(4), p 634
8. E. Shearier, P.K. Bowen, W. He, A. Drelich, J. Drelich, J. Goldman, and F. Zhao, In vitro Cytotoxicity, Adhesion, and Proliferation of Human Vascular Cells Exposed to Zinc, *ACS Biomater. Sci. Eng.*, 2016, **2**(4), p 634
9. P.K. Bowen, R. Guillory, E.R. Shearier, J.M. Seitz, J. Drelich, M.L. Bocks, F. Zhao, and J. Goldman, Metallic Zinc Exhibits Optimal Biocompatibility for Bioabsorbable Endovascular Stents, *Mater. Sci. Eng., C*, 2015, **56**, p 467
10. N.S. Murni, M.S. Dambatta, S.K. Yeap, G.R.A. Froemming, and H. Hermawan, Cytotoxicity Evaluation of Biodegradable Zn-3 Mg Alloy Toward Normal Human Osteoblast Cells, *Mater. Sci. Eng., C*, 2015, **49**, p 560–566
11. M. Sikora-Jasinska, E. Mostaed, A. Mostaed et al., Fabrication, Mechanical Properties and in Vitro Degradation Behavior of Newly Developed ZnAg Alloys for Degradable Implant Applications, *Mater. Sci. Eng., C*, 2017, **77**, p 1170–1181
12. J.S. Jing, T.M. Wang, R. Ling, and Y. Ke, The Beneficial Effects of Copper in the Cardiovascular System, *Adv. Mod. Biomed.*, 2018, **18**(16), p 3196–3200
13. Y. Ke and R. Ling, New Copper-Containing Metal Cardiovascular Scaffold Materials, *Progress Chin. Mater.*, 2018, **37**(09), p 681–692
14. Y. Ma. Research on Copper-based Solder Brazing Particle Reinforced Composite Coating, 2007
15. Z.B. Tang, J.L. Niu, H. Huang, H. Zhang, J. Pei, J. Pei, and G.Y. Yuan, Potential Biodegradable Zn-Cu Binary Alloys Developed for Cardiovascular Implant Applications, *J. Mech. Behav. Biomed. Mater.*, 2017, **72**, p 182–192
16. D. Gerlier and N. Thomasset, Use of MTT Colorimetric Assay to Measure Cell Activation, *J. Immunol. Methods*, 1986, **94**(1–2), p 57–63
17. S. Zhang, X. Zhang, C. Zhao, J. Li, Y. Song, C. Xie, H. Tao, Y. Zhang, Y. He, Y. Jiang, and Y. Bian, Research on an Mg-Zn Alloy as a Degradable Biomaterial, *Acta Biomater.*, 2010, **6**, p 626–640
18. X. Zhang, G. Yuan, L. Mao, J. Niu, P. Fu, and W. Ding, Effects of Extrusion and Heat Treatment on the Mechanical Properties and Biocorrosion Behaviors of a Mg-Nd-Zn-Zr Alloy, *Mech. Behav. Biomed. Mater.*, 2012, **7**, p 77–86
19. S. Lin, Q. Wang, X. Yan et al., Mechanical Properties, Degradation Behaviors and Biocompatibility Evaluation of a Biodegradable Zn-Mg-Cu Alloy for Cardiovascular Implants, *Mater. Lett.*, 2019, **234**, p 294–297
20. J. Wang, F. Witte, T. Xi, Y. Zheng, K. Yang, Y. Yang, D. Zhao, J. Meng, Y. Li, W. Li, K. Chan, and L. Qin, Recommendation for Modifying Current Cytotoxicity Testing Standards for Biodegradable Magnesium-Based Materials, *Acta Biomater.*, 2015, **21**, p 237–249